

TYPE I X-RAY BURSTS FROM THE NEUTRON-STAR TRANSIENT XTE J1701–462

DACHENG LIN¹, DIEGO ALTAMIRANO², JEROEN HOMAN¹, RONALD A. REMILLARD¹, RUDY WIJNANDS², AND TOMASO BELLONI³¹ MIT Kavli Institute for Astrophysics and Space Research, MIT, 70 Vassar Street, Cambridge, MA 02139-4307, USA; lindc@mit.edu² Astronomical Institute, “Anton Pannekoek,” University of Amsterdam, and Center for High Energy Astrophysics, Kruislaan 403, 1098 SJ Amsterdam, Netherlands³ INAF-Osservatorio Astronomico di Brera, Via E. Bianchi 46, I-23807 Merate (LC), Italy

Received 2009 February 5; accepted 2009 April 22; published 2009 June 9

ABSTRACT

The neutron-star X-ray transient XTE J1701–462 was observed for ~ 3 Ms with *RXTE* during its 2006–2007 outburst. Here we report on the discovery of three type-I X-ray bursts from XTE J1701–462. They occurred as the source was in transition from the typical Z-source behavior to the typical atoll-source behavior, at $\sim 10\%$ of the Eddington luminosity. The first burst was detected in the Z-source flaring branch (FB); the second in the vertex between the FB and normal branches; and the third in the atoll-source soft state. The detection of the burst in the FB cast doubts on earlier speculations that the FB is due to unstable nuclear burning of accreted matter. The last two of the three bursts show photospheric radius expansion, from which we estimate the distance to the source to be 8.8 kpc with a 15% uncertainty. No significant burst oscillations in the range 30–4000 Hz were found during these three bursts.

Key words: stars: distances – stars: neutron – X-rays: binaries – X-rays: bursts

1. INTRODUCTION

As accreted H/He-rich matter accumulates on the surface of a neutron star (NS), it is compressed and heated, occasionally leading to violent thermonuclear burning, a phenomenon known as type I X-ray bursts. Such bursts were discovered during the mid-1970s (Grindlay et al. 1976; Belian et al. 1976), and many theoretical studies have been made to investigate their detailed properties (e.g., Joss 1977; Lamb & Lamb 1978; Narayan & Heyl 2003; Woosley et al. 2004; Cooper & Narayan 2006). For reviews, see Lewin et al. (1993), Cumming (2004), and Strohmayer & Bildsten (2006). Recently, Galloway et al. (2008) presented a large sample of bursts (1187 in total) observed by *RXTE* over a time interval of more than 10 years.

The bursts typically rise very rapidly (< 2 s), followed by a slower exponential decay (~ 10 s to several minutes). The burst spectra can be fit with a single blackbody (BB) (Swank et al. 1977; Hoffman et al. 1977; Galloway et al. 2008). Burst properties do depend on the mass accretion rate (\dot{m}) and the composition of the accreted matter (see Table 1 by Galloway et al. (2008), and references therein and above). Roughly, for solar metallicities, the bursts mostly burn helium and have a fast rise when \dot{m} is about 1%–10% of the Eddington limit (\dot{m}_{Edd}). At higher or lower \dot{m} , they burn mixed hydrogen and helium and have a slower rise and decay. If the accreted matter is dominated by helium, the bursts mostly burn helium, and their properties vary little with the accretion rate. The accreted matter is expected to burn stably at \dot{m} close to or above \dot{m}_{Edd} (although bursts are seen in some Z sources, see below). In bright bursts, the photospheric layer can be lifted off the NS surface by radiation pressure when the local X-ray luminosity reaches the Eddington limit. Under certain assumptions, these bursts can then be used as distance estimators (Basinska et al. 1984; Kuulkers et al. 2003; Galloway et al. 2003).

Bursts are only found in weakly magnetized NS X-ray binaries, which mainly consist of two classes, i.e., atoll and Z sources (Hasinger & van der Klis 1989; van der Klis 2006). They have different luminosity, spectral and timing properties, etc. Atoll sources have \dot{m} typically $< 0.5\dot{m}_{\text{Edd}}$ and can have hard and soft states in addition to the transition between them. In the hard state, a significant fraction of the energy is emitted

above 20 keV and is normally accompanied by radio jets (e.g., Fender 2006; Migliari & Fender 2006). The source in the soft state has relatively much weaker emission above 20 keV and is believed to be dominated by emission from the accretion disk and the boundary layer where the accreted matter impacts the NS surface. Bursts are very often seen in atoll sources and have been observed in any of the above X-ray states (e.g., Galloway et al. 2008).

Z sources include six classical objects Sco X-1, GX 17+2, GX 349+2, Cyg X-2, GX 340+0, and GX 5-1 (Hasinger & van der Klis 1989), with \dot{m} close to or above \dot{m}_{Edd} . In the color-color diagram, Z sources can trace out a “Z” pattern, whose branches are called horizontal, normal, and flaring branches (HB/NB/FB), respectively. The Z pattern can move in the diagram, most obviously in the case of Cyg X-2. Although the spectra in Z sources are all soft and dominated by the emission from the accretion disk and boundary layer, these branches are different from each other in spectral and timing properties and evolution timescales. Only GX 17+2 has exhibited type I X-ray bursts, and no bursts have been reported to be in the FB (Kahn & Grindlay 1984; Tawara et al. 1984; Sztajno et al. 1986; Kuulkers et al. 2002). There are burst events in Cyg X-2, but their thermonuclear origin is still inconclusive (Kuulkers et al. 1995; Wijnands et al. 1997; Galloway et al. 2008).

In this paper, we report an analysis of X-ray bursts from the NS X-ray binary XTE J1701–462 during its 2006–2007 outburst. XTE J1701–462 is a unique source in that it is the first NS transient that shows Z-source characteristics (Homan et al. 2007c; Lin et al. 2009). During the decay of the outburst, the source changed from the typical Z-source behavior to the typical atoll-source behavior (Lin et al. 2009; J. Homan et al. 2009, in preparation). The analyses of comprehensive pointed observations of this outburst by *RXTE* have improved our understanding of atoll and Z sources and the physical processes associated with the three Z-source branches. For example, the spectral analysis in Lin et al. (2009) showed that the evolution from the Z to atoll sources and the movement of the “Z” tracks for Z sources in the color-color diagram result from the change in \dot{m} . The three Z-source branches were also suggested to represent three distinct physical mechanisms presumably operating at constant \dot{m} . Our analysis of

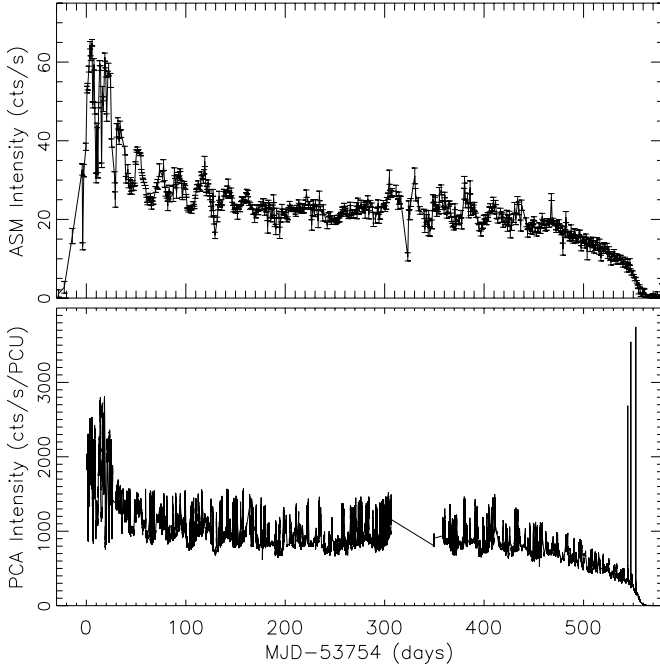


Figure 1. One-day ASM light curve (upper panel) and 32 s PCA light curve (lower panel). The three prominences in the decay of the PCA light curve are type I X-ray bursts, where 1 s data are used.

its bursts is another part of our campaign to understand this source.

Preliminary results of the bursts from XTE J1701–462 have been given in Homan et al. (2007a, 2007b) and Lin et al. (2007). In Section 2, we first carry out a systematic search of the *RXTE* archive for bursts from this source. We then present the spectral fit results of the bursts and estimate the distance of this source in Section 3. We describe our search for burst oscillations in Section 4. Finally we discuss our results and summarize our conclusions in Section 5.

2. OBSERVATIONS AND BURST SEARCH

We carried out a systematic search for bursts from XTE J1701–462 during its 2006–2007 outburst. We used all 866 pointed observations (~ 3 Ms) of XTE J1701–462 made with the Proportional Counter Array (PCA; Jahoda et al. 1996) on board *RXTE*. We used the same scheme as that used by Remillard et al. (2006), which is briefly described as follows. PCA 1 s light curves were created for each observation from “standard1” data mode, which integrates over the full energy range of the instrument (effectively 2–40 keV). For a time bin t , with intensity $C(t)$, we computed the mean b_1 and the sample standard deviation σ_1 using 1 s data in a “background” interval $t - 280$ to $t - 20$ and the corresponding values (b_2 and σ_2) in another “background” interval $t + 180$ to $t + 280$ after it. Then we tested the joint condition $[C(t) - b_1] > 5\sigma_1$ and $[C(t) - b_2] > 5\sigma_2$. If this condition is satisfied for three sequential data points (at $t - 1$, t , and $t + 1$), then we claim to find a burst candidate at t . Candidates are rejected if they are due to detector breakdowns; see http://heasarc.gsfc.nasa.gov/docs/xte/recipes/pca_breakdown.html for more information.

Using the above scheme we find three burst candidates. They are on 2007 July 17, 20, and 25, during observations 93703–01–01–01, 93703–01–02–00, and 93703–01–02–08. We number them I, II, and III, respectively (see Table 1 for details). All three

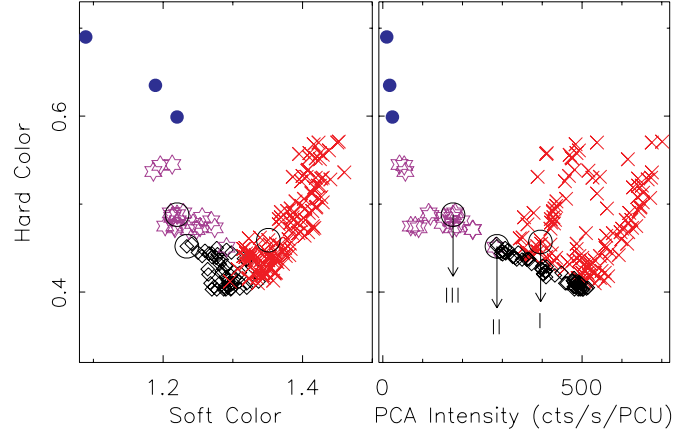


Figure 2. Color-color and hardness-intensity diagrams for observations between MJD 54260 and 54315 in the decay of the 2006–2007 outburst of XTE J1701–462. Blue filled circles for atoll-source hard state, purple hexagrams for atoll-source soft state, red crosses for Z-source flaring branch and, black diamonds for the normal/flaring branch vertex. The circled points mark the location of the bursts. The data binsize is 960 s, but longer for observations in the atoll-source soft and hard states (see the text).

bursts have the above condition satisfied for ~ 20 sequential data points. The upper panel of Figure 1 shows the 1-day light curve from the All-Sky Monitor (ASM; Levine et al. 1996), while the lower panel shows the 32 s light curve from the Proportional Counter Unit (PCU) 2 of the PCA, with 1 s bin size used for the three observations with bursts detected to show these bursts more clearly. The three bursts occur around the transition of XTE J1701–462 from the stage characteristic of a Z source to that of an atoll source.

Figure 2 shows the color-color diagram and hardness-intensity diagram for observations from Modified Julian Day (MJD) 54260 to 54315 in the decay of the outburst. The soft color and hard color are the count rate ratios in the (3.6–5.0)/(2.2–3.6) keV bands and the (8.6–18.0)/(5.0–8.6) keV bands, respectively. Each data point has an integration time ~ 960 s for observations before MJD 54304, but corresponds to an entire observation for later observations, which show little spectral variability. Several observations are further combined when intensity is < 30 counts s^{-1} PCU $^{-1}$. The figure is symbol-coded: blue filled circles for atoll-source hard state, purple hexagrams for atoll-source soft state, red crosses for Z-source FB, and black diamonds for the transition between the Z-source NB and the FB (NB/FB vertex). The classification of the states/branches is from Lin et al. (2009).

During the time interval for data shown in Figure 2, the source is not observed to enter the Z-source NB or HB. The FB in this interval shows the same spectral evolution and timing properties as the FB at higher luminosity when all Z-source branches were observed (Lin et al. 2009; J. Homan et al. 2009, in preparation). Given the shape of the color track shown in Figure 2 and in view of the low persistent luminosity ($\sim 10\%$ of L_{Edd} , see below), one could also classify the FB in Figure 2 as the atoll-source upper banana branch. The evolution of the color tracks shown in Lin et al. (2009) and J. Homan et al. (2009, in preparation) suggests that the atoll-source upper banana branch and the Z-source FB as defined by Hasinger & van der Klis (1989) describe a similar phenomenon, albeit at different luminosities. In this paper, we will follow the state/branch classification scheme by Lin et al. (2009), in which the Z-source FB phenomenon can be observed down to luminosities typically associated with atoll sources.

Table 1
Three Bursts from XTE J1701–462 Observed by *RXTE*

Burst Number		I	II	III
Observation ID		93703–01–01–01	93703–01–02–00	93703–01–02–08
Persistent emission	Count rate (counts s ⁻¹ PCU ⁻¹)	396	301	176
	Soft color	1.35	1.28	1.22
	Hard color	0.46	0.44	0.49
	Source branch/state ^a	FB	NB/FB vertex	atoll SS
	Flux (2.5–25 keV, 10 ⁻⁹ erg cm ⁻² s ⁻¹)	4.45 ± 0.07	3.38 ± 0.04	1.99 ± 0.02
	Flux (bolometric, 10 ⁻⁹ erg cm ⁻² s ⁻¹)	6.17 ± 0.12	4.90 ± 0.10	2.94 ± 0.05
Burst ^b	Dimensionless flux γ	0.150 ± 0.004	0.119 ± 0.003	0.072 ± 0.002
	Start time (UT)	2007/07/17 12:24:22	2007/07/20 14:14:04	2007/07/25 13:39:24
	Rise time (s)	0.5	1.5	1.5
	Decay timescale τ_1 (s)	4.1 ± 0.3	2.6 ± 0.2	3.4 ± 0.3
	Decay timescale τ_2 (s)	10.6 ± 5.0	5.6 ± 1.9	8.5 ± 4.7
	Characteristic timescale τ (s)	5.6 ± 0.2	5.5 ± 0.2	6.4 ± 0.2
	Peak count rate (counts s ⁻¹ PCU ⁻¹)	2248	3382	3465
	Peak flux (10 ⁻⁹ erg cm ⁻² s ⁻¹)	27.2 ± 1.0	39.2 ± 1.1	42.9 ± 1.2
	Fluence (10 ⁻⁷ erg cm ⁻²)	1.52 ± 0.03	2.16 ± 0.03	2.76 ± 0.04
	Asymptotic radius (km, at 8.8 kpc)	7.9 ± 1.5	8.0 ± 1.6	7.9 ± 1.3
	Radius expansion?	N	Y	Y
	Pulsed fraction upper limit	37.9%	14.6%	51.4%

Notes.

^a The source branch/state classification is from Lin et al. (2009). FB: flaring branch; NB/FB vertex: the transition between the normal and flaring branches; atoll SS: atoll-source soft state.

^b Persistent emission subtracted.

In Figure 2, we circle the data points where the bursts are detected. Burst I is in the FB, burst II in the NB/FB vertex, and burst III in the atoll-source soft state. The persistent emission stays roughly constant for the observations when bursts II and III are observed, and the occurrences of the bursts seem not to modify the persistent emission. We examine the same question in greater detail for the observation containing burst I (Obs 93703–01–01–01), since this is the first occurrence of a burst from a Z source while it is in the FB. In order to see whether the persistent emission is modified by the burst, especially to see whether the source jumps to the NB/FB vertex right after the burst, we show in Figure 3 the hardness-intensity diagram for this observation (red crosses). Results for the next adjacent observation (Obs ID 93703–01–01–08; about 1 day later), when the source is in the NB/FB vertex, are also shown (black diamonds) for comparison. Data points with 32 s bin size are used. The two data points in the triangles are from the interval containing burst I. The data points are connected by black solid lines in time to show the source evolution. We clearly see that the source stays roughly at the same position in this diagram before and after the burst. From this we conclude that this burst does not interfere with the persistent emission in the FB either. Ramifications for this result are considered in Section 5.

The count rate, soft color, hard color, and flux of the persistent emission are given in Table 1. The flux is estimated using a model of a multi-color disk plus a single-temperature BB (Lin et al. 2009), with both 2.5–25 keV and bolometric values given (unabsorbed). The bolometric flux is obtained analytically as our model consists of two thermal components. The conversion of flux to luminosity is complicated by uncertainties in several important parameters, such as the source distance, the disk inclination and the occultation factor of the BB, and is therefore not carried out here. Instead, we give in Table 1 the dimensionless flux (γ ; van Paradijs et al. 1988), i.e., the ratio of the bolometric persistent flux to the Eddington flux inferred from the radius expansion bursts (see below). Based on this parameter, the \dot{m} when the bursts are detected is roughly 10% of \dot{m}_{Edd} .

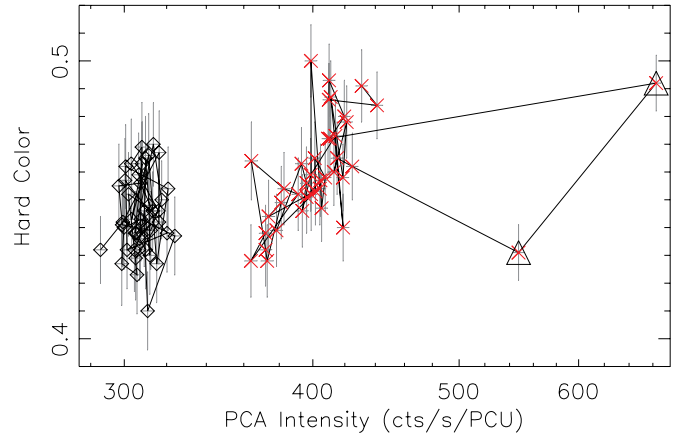


Figure 3. Hardness-intensity diagram for observations 93703–01–01–01 and 93703–01–01–08 using 32 s data. Black diamonds are for the Z-source normal/flaring branch vertex and are all from observation 93703–01–01–08, and red crosses for Z-source flaring branch and all from observation 93703–01–01–01. The two data points in the triangles are from the interval containing the bursts. We connect the time-series data points with solid lines to show the source evolution. The 1 σ error bars for the hard color and intensity are also shown, with gray lines.

3. BURST SPECTRAL FITS

We used a standard procedure to do spectral fits of the three bursts: create time-resolved spectra, use the persistent emission around the burst as background, and fit the spectra with a BB model (e.g., Galloway et al. 2008). We used a 15 s interval that ended 35 s before the burst to define the persistent emission. Event mode data with 64 channels and 125 μ s time resolution were used. Only PCUs 0 and 2 were on during the observations in which the above three bursts were detected. Considering that the spectral calibration of PCU 0 has been bad at energies lower than 10 keV since the loss of the propane layer in 2000, we only used data from PCU 2. We note that Lin et al. (2007) used data from both PCUs. The peak count rates of these bursts are quite high

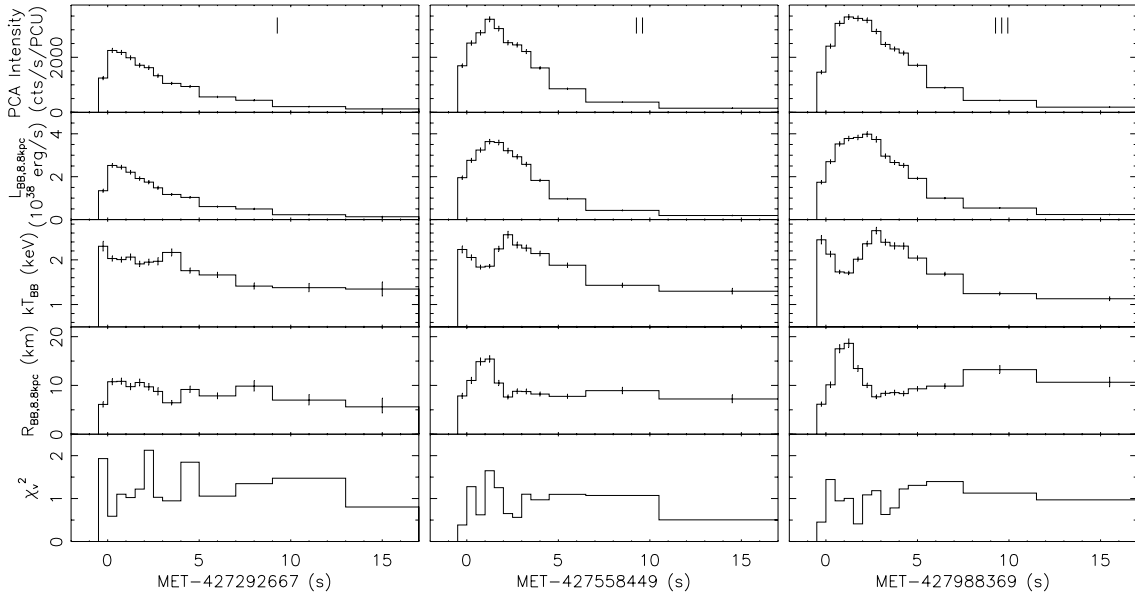


Figure 4. Results of the spectral fits of time-resolved spectra of the three bursts detected from XTE J1701–462 during its 2006–2007 outburst. The latter two bursts show photospheric radius expansion.

(~ 3500 counts/s/PCU), but by comparing with the count rates from “standard1” mode data, we found no telemetry saturation in the event mode data. The integration time of the spectra was set to be 0.5 s around the peak and increased as the count rate decreased to maintain sufficient statistics to constrain the spectral parameters. An energy range of 3.5–20 keV was used, and 0.8% systematic errors were applied. Deadtime corrections, which were as large as 5%, were also made as suggested by *RXTE* team. The response files were created using HEASoft version 6.4. A hydrogen column density $N_H = 2.0 \times 10^{22} \text{ cm}^{-2}$ was assumed; it was inferred from spectral fitting of the persistent emission using simultaneous observations of *RXTE* and *Swift*/XRT (Lin et al. 2009), and is consistent with the value inferred from fitting of quiescence spectra (J. Fridriksson et al. 2009, in preparation).

The results of our spectral fits are shown in Figure 4. There are five panels for each burst (all with persistent emission background subtracted); PCA intensity, bolometric luminosity, BB temperature kT_{BB} , BB radius R_{BB} , and reduced χ^2 are all shown versus time. The luminosity and radius were calculated at a distance of 8.8 kpc (see below). The low values of reduced χ^2 suggest that the net burst spectra are well fit by a BB. The fast rise and slow cooling decay confirm that these bursts are bona fide type I X-ray bursts.

The most important feature that Figure 4 shows is that the two brightest bursts (II and III) show photospheric radius expansion, as indicated by the anti-correlation between the temperature and radius when the luminosity reaches its peak: the temperature decreases from ~ 2.5 keV to ~ 1.8 keV while the radius increases from ~ 10 km to ~ 20 km. Radius expansion bursts are also often studied in terms of the BB luminosity versus the temperature, as shown in Figure 5. In this figure, the arrows indicate the direction of the temporal evolution. As shown in the panels for bursts II and III, the source tends to evolve along a horizontal line (constant luminosity) during the radius expansion/contraction phase but along a (dashed) diagonal line (constant radius) during the cooling decay phase.

We use these radius expansion bursts to estimate the distance to XTE J1701–462. The peak flux in bursts II and III are given in Table 1 with an average value of $41.1 \pm 0.8 \times 10^{-9} \text{ erg cm}^{-2}$

s^{-1} . Using the empirically determined Eddington luminosity $3.79 \pm 0.15 \times 10^{38} \text{ erg s}^{-1}$ for bursts showing photospheric radius expansion (Kuulkers et al. 2003, with uncertainty 15%), we derive a distance of 8.8 kpc. Using a theoretical expression for the Eddington limit (see Equation (8) in Galloway et al. 2008) and assuming a 1.4 solar-mass NS with a radius of 10 km, we obtain a distance of 7.3 ± 0.1 kpc for H-poor case (H-fraction $X = 0$) and 5.6 ± 0.1 kpc for H-rich case ($X = 0.7$). We assumed that the peak luminosity is reached when the photosphere has settled back on the NS surface (Galloway et al. 2008), which is roughly true in this case (Figure 4). Hereafter, we use the value derived by the empirical method, i.e., 8.8 kpc.

The other properties of the bursts are listed in Table 1. The start time was defined to be the time when the burst flux first exceeded 25% of the peak flux, and the rise time is the interval that it takes for the burst flux to increase from 25% to 90% of the peak value (Galloway et al. 2008). We see that all three bursts rise very rapidly, i.e., within ~ 1 s. Such bursts are probably due to Helium burning, which is consistent with the \dot{m} ($\sim 10\%$ of \dot{m}_{Edd}) during these bursts (Section 1). The bursts show exponential decays but cannot be fit with a single exponential curve. Thus, as in Galloway et al. (2008), we divide the decay (using the bolometric flux curve) into two parts and fit each with an exponential curve with independent decay constants τ_1 and τ_2 . These bursts decay rapidly, on timescales of several seconds. The fluence in Table 1 is estimated by summing the fluxes over the burst and integrating the final exponential curve to account for the additional flux beyond the data window. The characteristic timescale τ is the fluence divided by the peak flux. It is ~ 6 s for all bursts.

As the bursts decay, the radius tends to remain at an asymptotic value, as also shown in Figure 5, and this is a signal of unstable nuclear burning in the bursts spreading over the whole NS surface (Lewin et al. 1993). We calculate the asymptotic radius in the burst tails using data when the burst flux decays from 80% to 20% of the peak value. The asymptotic radius for each burst is also listed in Table 1 with an average of 8 ± 1 km at a distance of 8.8 kpc (corresponding to the dashed line in Figure 5). We note that there is a slight increase in emission area in burst III as the decay progresses, as can be seen in

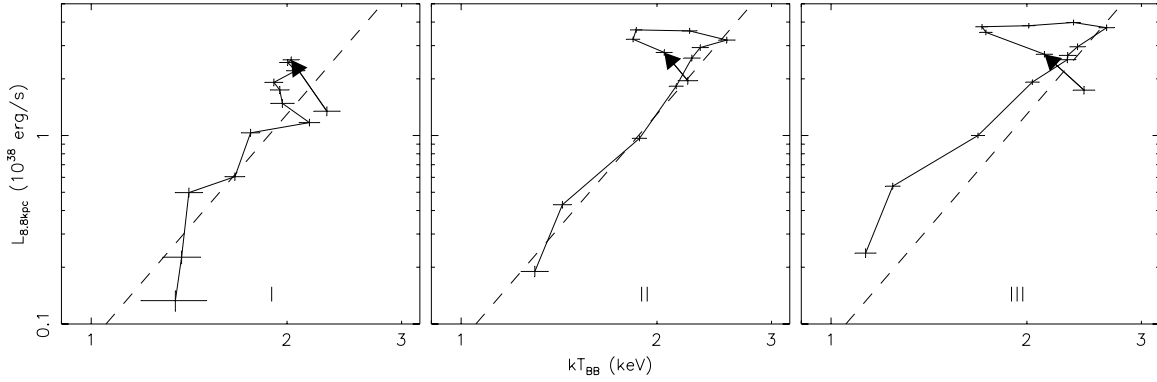


Figure 5. Burst luminosity vs. blackbody temperature. The arrows show the direction of burst evolution. The dashed lines correspond to $R_{\text{BB}} = 8$ km.

Figure 5, the cause of which is unknown. The effects of redshift and spectral hardening should be corrected for in order to obtain the actual size of the NS (Lewin et al. 1993). If a 1.4 solar-mass NS and a hardening factor of 1.4 (e.g., Madej et al. 2004) are assumed, then the actual size of the NS is ~ 13 km.

4. BURST OSCILLATION SEARCH

We searched each burst for coherent pulsations in the frequency range 30–4000 Hz using Fourier techniques. We computed power spectra throughout each burst using sliding 1, 2, 3, and 4 s windows with a step of 0.125 s. The investigated energy bands were 2–60, 2–10, and 10–30 keV. We found no significant signal. To estimate the upper limits, we used the set of Leahy-normalized power spectra (Leahy et al. 1983) with a 1 s window so as to take into account possible frequency drifts.

The upper limit for each burst was then determined as follows (see also Vaughan et al. 1994): (1) we searched for the largest observed power P_{max} in the 2–60 keV band, (2) we fit the noise powers of the power spectrum in which we found P_{max} with a constant plus power law model, (3) we divided by the continuum model and multiplied by 2 to re-normalize the power spectrum (see e.g., Israel & Stella 1996; Watts & Strohmayer 2006), and (4) we estimated the upper limits at a 99% confidence level using the Groth distribution (Groth 1975; Vaughan et al. 1994). The pulsed fraction upper limits are listed in Table 1. They are relatively high and not very constraining, compared with the typically observed amplitudes of oscillations of a few 10% (Strohmayer & Bildsten 2006).

5. DISCUSSIONS AND CONCLUSIONS

We find three type I X-ray bursts from the 866 *RXTE* pointed observations (~ 3 Ms) of the NS transient XTE J1701–462 during its 2006–2007 outburst. These bursts are detected during the decay of the outburst. The persistent emission of the observations containing these three bursts is weak, with fluxes $\sim 10\%$ of the Eddington limit. Based on the source state/branch classifications by Lin et al. (2009), the first burst is detected in the Z-source FB; the second in the FB/NB vertex; and the third in the atoll-source soft state.

Detailed spectral fits confirm these bursts as type I X-ray bursts. The last two of the three bursts show strong photospheric radius expansion with a peak flux of $41.1 \pm 0.8 \times 10^{-9}$ erg $\text{cm}^{-2} \text{s}^{-1}$. Assuming an Eddington luminosity of $3.79 \pm 0.15 \times 10^{38}$ erg s^{-1} (Kuulkers et al. 2003), we estimate a distance of 8.8 kpc for XTE J1701–462 with 15% systematic uncertainty. We find no significant burst oscillations between 30–4000 Hz.

The distance to XTE J1701–462 was initially estimated by Homan et al. (2007c). They gave a distance of 14.7 ± 3 kpc by comparing the flux in the NB/FB vertex in a Sco-like Z-source interval with that of Sco X-1 (which has a distance of 2.8 ± 0.3 kpc, as determined by radio parallax measurements). This value is higher than that derived here using radius expansion bursts. A possible explanation for such a discrepancy is a difference in the inclination of these two systems. The orbital inclination of Sco X-1 is $\sim 40^\circ$ (Fomalont et al. 2001; Steeghs & Casares 2002). The above discrepancy can be explained if XTE J1701–462 has orbital inclination of 70° , as roughly estimated by Lin et al. (2009) based on the weak iron emission lines detected, assuming that the flux is dominated by the disk emission.

The occurrence of the burst near the end of the outburst is consistent with the behavior of XTE J1701–462 changing to that typical of an atoll source. Atoll sources are known to be much more prolific bursters than Z sources. Among the six classical Z sources, only GX 17+2 has exhibited type I X-ray bursts (Section 1). These sources accrete at high \dot{m} , close to or above \dot{m}_{Edd} , as inferred from its radius expansion bursts. GX 17+2 has both short ($\tau \lesssim 10$ s) and long ($\tau > 100$ s) bursts. Burst-like events from Cyg X-2 are very short ($\tau \sim 3$ s), and many of them do not show cooling during burst decay. Thus their thermonuclear origin is inconclusive (Kuulkers et al. 1995; Wijmans et al. 1997; Galloway et al. 2008). XTE J1701–462 is different in that its bursts are detected when it accretes at low \dot{m} , $\sim 10\%$ of \dot{m}_{Edd} and that all bursts are short ($\tau \sim 6$ s). From the \dot{m} and the burst profiles (fast rise and short duration), these bursts are consistent with helium burning. Such bursts are often seen in the atoll sources in their banana branch (Galloway et al. 2008). Thus the unstable nuclear burning in these bursts should fall under the framework of the classical burst theory, indicating that Z sources can have regular bursts. The results that these bursts are consistent with helium burning can also be explained if the NS is accreting H-poor material, as is often seen in ultra-compact X-ray binaries, which have orbital periods of an hour or less and have helium accreted from a degenerate donor. There is no optical spectrum of the mass donor in XTE J1701–462 to determine whether it is H-poor. However, the 2006–2007 outburst is very long (~ 20 months), while ultra-compact X-ray binaries have never displayed such long outbursts when their light curves can be associated with the class of soft X-ray transients. Thus the mass donor in XTE J1701–462 is probably a normal star transferring H-rich material.

So far no bursts have been detected in the FB (except in the NB/FB vertex) from GX 17+2 (Kuulkers et al. 2002), while the thermonuclear origin of the burst-like events from

Cyg X-2 is inconclusive (see references above). While the detection of burst I from XTE J1701–462 in a low luminosity FB might not be unique, given the abundance of burst in the atoll upper banana branch (Galloway et al. 2008), it does cast doubt on the speculation that the Z-source FB is caused by unstable nuclear burning (Church et al. 2006). In Section 2, we show that burst I does not interfere with the FB behavior, in that no jump in the hardness-intensity diagram is seen before and after the burst. In Section 3, we also show that burst I should have spread over the whole NS surface, since there is constant emission area during the decay. Thus, considering that the FB and bursts are different (e.g., bursts rise in seconds, but the FB rises in minutes or longer), if the FB is caused by unstable nuclear burning, it must be a different type of nuclear burning from that for bursts, and it can coexist when burst I burns nuclear material globally in XTE J1701–462. Although we cannot simply exclude a complex environment allowing the above scenario, current theoretic studies do not favor coexistence of two types of unstable nuclear burning (e.g., Heger et al. 2007). Thus the explanation of unstable nuclear burning for the FB is quite uncertain. Lin et al. (2009) offered an additional argument that the FB cannot be due to unstable nuclear burning, as the energy released to produce the FB would require a much higher \dot{m} than is observed. Lin et al. (2009) propose an alternative explanation for the FB, in which the inner disk radius contracts temporarily from an Eddington-expanded value toward the innermost stable circular orbit.

The burst rate depends on \dot{m} and is expected to be zero at \dot{m} close to \dot{m}_{Edd} (Remillard et al. 2006; Galloway et al. 2008). While this is consistent with the fact that we do not observe bursts during the bright phase of the outburst for XTE J1701–462 and in most of Z sources, it does raise the question of why the Z source GX 17+2 shows type-I X-ray bursts. One possible explanation could be that bursts are possible at high \dot{m} , but only in the narrow \dot{m} -range occupied by GX 17+2. We test this hypothesis by estimating the expected number of bursts from XTE J1701–462, for the duration when it was similar to GX 17+2. We estimate that XTE J1701–462 has ~ 0.5 Ms of exposure when it resembles GX 17+2, i.e., with all three Sco-like Z branches traced out, and thus has a similar \dot{m} as well. However, XTE J1701–462 has no burst detected in this ~ 0.5 Ms interval, while we would have expected to see ~ 6 bursts, based on the burst rate of GX 17+2 (12 bursts observed in 1 Ms with *RXTE* (Galloway et al. 2008)). Thus the burst rate in GX 17+2 is much higher than XTE J1701–462 at similar \dot{m} . It suggests that bursts in GX 17+2 are not only due to its specific \dot{m} , but might also depend on other factors such as the NS parameters or the chemical composition of the accreted matter.

The three bursts are detected at $\dot{m} \sim 10\% \dot{m}_{\text{Edd}}$, with the burst rate about 1 per 10 hr, considering that the source is observed for several tens of hours around such \dot{m} . This is consistent with the average value, ~ 12 hr from Galloway et al. (2008) or ~ 6 hr from Remillard et al. (2006), corresponding to the above \dot{m} .

This research has made use of data obtained from the High Energy Astrophysics Science Archive Research Center (HEASARC), provided by NASA's Goddard Space Flight Center. T.B. acknowledges support from ASI through grant I/088/06/0.

REFERENCES

- Basinska, E. M., Lewin, W. H. G., Sztajno, M., Cominsky, L. R., & Marshall, F. J. 1984, *ApJ*, **281**, 337
- Belian, R. D., Conner, J. P., & Evans, W. D. 1976, *ApJ*, **206**, L135
- Church, M. J., Halai, G. S., & Bałucińska-Church, M. 2006, *A&A*, **460**, 233
- Cooper, R. L., & Narayan, R. 2006, *ApJ*, **652**, 584
- Cumming, A. 2004, *Nucl. Phys.*, **132**, 435
- Fender, R. 2006, in *Compact Stellar X-ray Sources*, ed. W. Lewin & M. van der Klis (Cambridge: Cambridge Univ. Press), **381**
- Fomalont, E. B., Geldzahler, B. J., & Bradshaw, C. F. 2001, *ApJ*, **558**, 283
- Galloway, D. K., Muno, M. P., Hartman, J. M., Psaltis, D., & Chakrabarty, D. 2008, *ApJS*, **179**, 360
- Galloway, D. K., Psaltis, D., Chakrabarty, D., & Muno, M. P. 2003, *ApJ*, **590**, 999
- Grindlay, J., et al. 1976, *ApJ*, **205**, L127
- Groth, E. J. 1975, *ApJS*, **29**, 285
- Hasinger, G., & van der Klis, M. 1989, *A&A*, **225**, 79
- Heger, A., Cumming, A., & Woosley, S. E. 2007, *ApJ*, **665**, 1311
- Hoffman, J. A., Lewin, W. H. G., & Doty, J. 1977, *ApJ*, **217**, L23
- Homan, J., Wijnands, R., Altamirano, D., & Belloni, T. 2007a, *The Astronomer's Telegram*, **1165**
- Homan, J., et al. 2007b, *The Astronomer's Telegram*, **1144**, 1
- Homan, J., et al. 2007c, *ApJ*, **656**, 420
- Israel, G. L., & Stella, L. 1996, *ApJ*, **468**, 369
- Jahoda, K., et al. 1996, *Proc. SPIE*, **2808**, 59
- Joss, P. C. 1977, *Nature*, **270**, 310
- Kahn, S. M., & Grindlay, J. E. 1984, *ApJ*, **281**, 826
- Kuulkers, E., et al. 2003, *A&A*, **399**, 663
- Kuulkers, E., Homan, J., van der Klis, M., Lewin, W. H. G., & Méndez, M. 2002, *A&A*, **382**, 947
- Kuulkers, E., van der Klis, M., & van Paradijs, J. 1995, *ApJ*, **450**, 748
- Lamb, D. Q., & Lamb, F. K. 1978, *ApJ*, **220**, 291
- Leahy, D. A., et al. 1983, *ApJ*, **266**, 160
- Levine, A. M., et al. 1996, *ApJ*, **469**, L33
- Lewin, W. H. G., van Paradijs, J., & Taam, R. E. 1993, *Space Sci. Rev.*, **62**, 223
- Lin, D., Homan, J., Remillard, R., & Wijnands, R. 2007, *The Astronomer's Telegram*, **1183**
- Lin, D., Remillard, R. A., & Homan, J. 2009, *ApJ*, **696**, 1257
- Madej, J., Joss, P. C., & Różańska, A. 2004, *ApJ*, **602**, 904
- Migliari, S., & Fender, R. P. 2006, *MNRAS*, **366**, 79
- Narayan, R., & Heyl, J. S. 2003, *ApJ*, **599**, 419
- Remillard, R. A., Lin, D., Cooper, R. L., & Narayan, R. 2006, *ApJ*, **646**, 407
- Steehls, D., & Casares, J. 2002, *ApJ*, **568**, 273
- Strohmayer, T., & Bildsten, L. 2006, in *Compact Stellar X-Ray Sources*, ed. W. Lewin & M. van der Klis (Cambridge: Cambridge Univ. Press), **113**
- Swank, J. H., et al. 1977, *ApJ*, **212**, L73
- Sztajno, M., et al. 1986, *MNRAS*, **222**, 499
- Tawara, Y., Hirano, T., Kii, T., Matsuoka, M., & Murakami, T. 1984, *PASJ*, **36**, 861
- van der Klis, M. 2006, in *Compact Stellar X-Ray Sources*, ed. W. Lewin & M. van der Klis (Cambridge: Cambridge Univ. Press), **39**
- van Paradijs, J., Penninx, W., & Lewin, W. H. G. 1988, *MNRAS*, **233**, 437
- Vaughan, B. A., et al. 1994, *ApJ*, **435**, 362
- Watts, A. L., & Strohmayer, T. E. 2006, *ApJ*, **637**, L117
- Wijnands, R. A. D., van der Klis, M., Kuulkers, E., Asai, K., & Hasinger, G. 1997, *A&A*, **323**, 399
- Woosley, S. E., et al. 2004, *ApJS*, **151**, 75